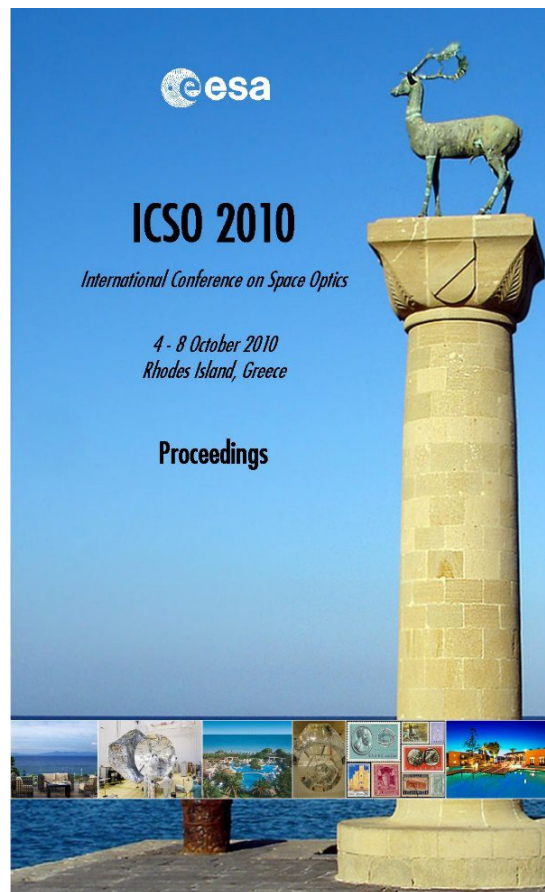


# International Conference on Space Optics—ICSO 2010

Rhodes Island, Greece

4–8 October 2010

*Edited by Errico Armandillo, Bruno Cugny,  
and Nikos Karafolas*



## *Performance characterization of the EarthCARE BBR Detectors*

*C. Proulx, M. Allard, T. Pope, B. Tremblay, et al.*



International Conference on Space Optics — ICSO 2010, edited by Errico Armandillo, Bruno Cugny,  
Nikos Karafolas, Proc. of SPIE Vol. 10565, 1056508 · © 2010 ESA and CNES  
CCC code: 0277-786X/17/\$18 · doi: 10.1117/12.2309219

## PERFORMANCE CHARACTERIZATION OF THE EARTHCARE BBR DETECTORS

C. Proulx<sup>1</sup>, M. Allard<sup>1</sup>, T. Pope<sup>1</sup>, B. Tremblay<sup>1</sup>, F. Williamson<sup>1</sup>, C. Julien<sup>1</sup>, C. Larouche<sup>1</sup>  
J. Delderfield<sup>2</sup>, D. Parker<sup>2</sup>.

<sup>1</sup>*Institut National d'Optique (INO), 2740, Einstein Street, Quebec, QC, G1P 4S4, Canada.*

<sup>2</sup>*Rutherford Appleton Laboratory (RAL), Harwell Science and Innovation Campus, DIDCOT, Oxfordshire,  
OX11 0QX, United Kingdom.*

### I. INTRODUCTION

The Broadband Radiometer (BBR) is an instrument being developed for the ESA EarthCARE satellite. The BBR instrument objective is to provide measurements of the reflected short-wave (0.25-4.0  $\mu\text{m}$ ) and emitted long-wave (4.0-50  $\mu\text{m}$ ) top of the atmosphere (TOA) radiance over three along-track views (forward, nadir and backward). The instrument has three fixed telescopes, one for each view, each containing a broadband detector. The BBR instrument is led by SEA in the UK with RAL responsible for the BBR optics unit (OU) while EADS Astrium is the EarthCARE prime contractor. A detailed description of the instrument is provided in [1].

The BBR detectors consist in three dedicated assemblies under the responsibility of INO. The detectors development started in 2008 and led to the design and implementation of a new gold black deposition facility at INO [2], in parallel with the preliminary and detailed design phases of the detector assemblies. As of today, two breadboard models and one engineering model have been delivered to RAL. In the BBR OU each detector mechanically interfaces with the telescope and electrically with the front-end electronics (FEE). The detectors' development is now at the Critical Design Review (CDR) level.

This paper first provides a description of the detector design along with its principles of operation. It further presents and discusses measurement and analysis results for the performance characterization of the engineering model in the context of the applicable requirements. Detector-level qualification planning is finally discussed.

### II. DETECTOR DESCRIPTION

The detectors are required to provide fast pixel response time ( $< 6$  ms), uniform spectral response over the entire spectral range (0.25-50  $\mu\text{m}$ ), and an NEP lower than 3.7 nW at 17 Hz (after time averaging over a period of 20 ms). The engineering model detector is shown in Fig. 1, with (right) and without (left) its cover.

Each detector consists of an uncooled focal plane array (FPA) hybridized with a readout integrated circuit (ROIC). The FPA is based on INO's  $\text{VO}_x$  microbolometer technology while the ROIC used is the XRO3501 by XenICs. The FPA is a linear array of 30 microbolometer pixels on a 100- $\mu\text{m}$  pitch, specially designed and fabricated for the BBR instrument [3]. The linear array is matched by an array of unsuspended (shunt) pixels such that each pair of pixels corresponds to a resistance half-bridge, which middle point is fed into the ROIC integrator input. This allows for compensation of the substrate temperature variation as the shunt pixels do not respond to the scene radiance. Furthermore, the FPA substrate temperature can be monitored by two additional thermometer pixels, one at each end of the linear array (both of which are directly fed into dedicated ROIC channels). The FPA linear array is covered with a gold black absorber in order to achieve the spectral uniformity required. The gold black layer is subsequently trimmed by laser micromachining to ensure individual pixel definition with a fill factor of at least 90% [3].

The FPA interfaces to the ROIC with a carrier chip that is used to compensate the different pad pitch of both dies and the circuit-card assembly (CCA). All interconnections are performed by use of aluminum-wire ultrasonic wedge-wedge bonding. The CCA provides basic electrical functions such as signal routing, decoupling and filtering, and is the primary interface to the instrument FEE through the unit's connector. The assembly is completed by a base-plate and (windowless) cover, which provide the mechanical and optical interfaces to the instrument telescope.

In the BBR instrument, the FEE provides separate voltages to the bolometric pixels ( $V_{\text{bolo}}$ ) and to the shunt pixels ( $V_{\text{shunt}}$ ) with respect to the ROIC reference voltage ( $V_{\text{ref}}$ , also provided by the FEE). The FEE also sets the ROIC gain parameters, namely the integrator capacitance ( $C_{\text{int}}$ ) and integration time ( $t_{\text{int}}$ ). The thermometer pixels (wired as single resistances directly to their respective ROIC input) are also biased by the FEE with a dedicated voltage ( $V_{\text{thermo}}$ ) with respect to the same reference voltage.

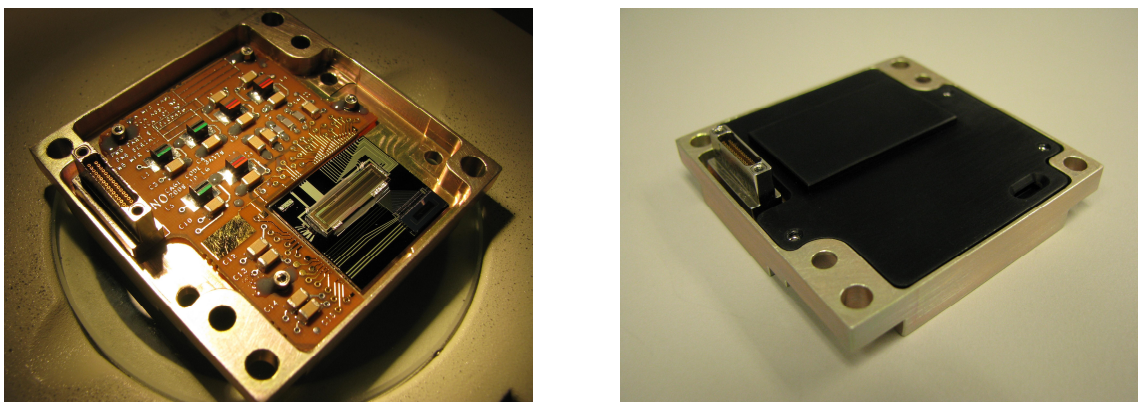


Fig. 1. BBR detector engineering model assembly

### III. ENGINEERING MODEL CHARACTERIZATION

Several development units were built and tested in order to support the detectors and instrument development, some being retained by INO for development purposes. This section presents experimental characterization of the engineering model (EM).

Testing of the detector units at INO is performed with a combination of custom-built ground support equipment (GSE) and commercial instrumentation. The unit under test is mounted in a thermal vacuum (TVAC) chamber equipped with an optical port. It is then connected to a custom electrical GSE assembly that emulates the instrument FEE by a dedicated feedthrough of the TVAC system. This GSE assembly supplies the constant bias voltages ( $V_{\text{bolo}}$ ,  $V_{\text{shunt}}$ ,  $V_{\text{thermo}}$ ) to the 30 active pixels and 2 thermometer pixels, and is used in conjunction with a XenICs XEVA camera that configures the ROIC settings ( $V_{\text{ref}}$ ,  $C_{\text{int}}$ ,  $t_{\text{int}}$ ) and reads the video output signal. The camera video output consists of a frame composed of 256 channel readings (of which only the 32 channels carrying a pixel signal are kept). The ROIC timing is set by the camera to be representative of the flight instrument.

For the tests described herein the detector scene is a blackbody located outside the TVAC chamber. The scene signal reaches the detector through the optical port. A shutter can be inserted between the detector and the scene if need be. A chopper is used in front of the blackbody to modulate its radiance. Optical filters can be used to further constrain the incident radiation on the detector. The irradiance at the detector can be determined by use of a reference measurement with a calibrated pyroelectric detector. The pyroelectric detector is assumed to have a flat spectral responsivity (the pyroelectric crystal is coated with an organic black coating). The test setup parameters (blackbody temperature, optical filter and distance between the detector and the scene) are adjusted to provide an optical power of  $1.1 \mu\text{W}$  incident on the FPA pixels (which corresponds to the BBR instrument dynamic range). Testing in some spectral channels requires that a lower optical power be used.

The EM test campaign was devised to meet the objectives of establishing an adequate test strategy for performance testing of subsequent units.

The first tests conducted consist in a sequence of verification that aims at validating the detector functionality and operability. For the test temperature considered (the EM was tested both at  $22^\circ\text{C}$  and  $-10^\circ\text{C}$ ), the ROIC transfer function is first characterized (the blackbody source is not required for this test). This is performed by setting  $V_{\text{bolo}}$  equal to  $V_{\text{ref}}$ , and by spanning  $V_{\text{shunt}}$  around the reference voltage until saturation is monitored at the video output. Several series of frames are acquired during this test for different values of  $V_{\text{shunt}}$  in order to plot the ROIC transfer function, and determine its linear range. A typical result is shown in Fig. 2, where the video output signal ( $V_{\text{mean}}$ ) is plotted against  $V_{\text{shunt}}$  for each of the 30 detector channels (excluding the thermometer pixel channels). For the EM, the best linearity is found at a video output ( $V_{\text{mean}}$ ) between 1.0 V and 4.0 V. We note that the maximum deviation between experimental points and a linear curve fit through those points (between 1.0 V and 4.0 V) is less than  $\pm 4 \text{ mV}$ . This measurement actually supports the verification of the linearity of the detector assembly, which is combined with an analytical validation (not presented here) that the bolometer pixels do not present resistance changes that are important enough to induce significant non-linearity over the instrument dynamic range. The specified detector linearity is important for the radiometric calibration of the BBR instrument.

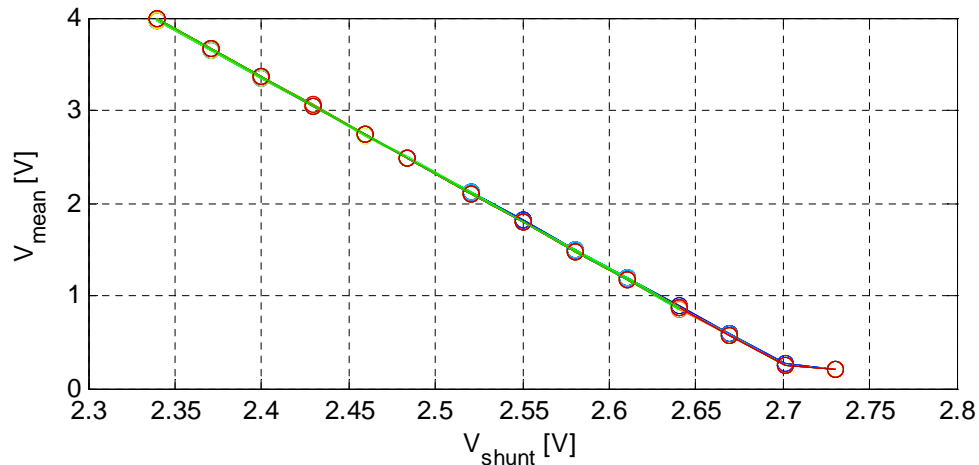


**Fig. 2.** Detector's ROIC transfer function measurement at  $-10^{\circ}\text{C}$

For the performance characterization, the EM unit was tested both at room temperature ( $22^{\circ}\text{C}$ ) and at the nominal instrument operating temperature ( $-10^{\circ}\text{C}$ ). For the tests at  $-10^{\circ}\text{C}$ , two sets of bias voltages were further used: the 'low-bias' set where the difference between  $V_{\text{bolo}}$  and  $V_{\text{ref}}$  was 1.4 V, and the 'high-bias' set where the difference between  $V_{\text{bolo}}$  and  $V_{\text{ref}}$  was 1.9 V. In all cases, the  $V_{\text{shunt}}$  voltage is adjusted and fixed so as to ensure that the detector response at the video output is within the ROIC linear range previously determined. There is a trade-off between the performance of the detectors (better responsivity and NEP is achieved for a higher bias) and their operation (a lower bias will be less sensitive to variations of the operational temperature), which needs to be performed at the instrument application level.

Fig. 3 presents the results for the NEP and responsivity characterization of the EM. The responsivity is determined by measuring the peak-to-peak response of the detector under a chopped blackbody radiation signal (at the instrument operational frequency of 17 Hz) that corresponds to the dynamic range of the instrument. Dividing this voltage response by the optical power incident on the detector pixels (reference measurement described above) yields the responsivity for each pixel. For the NEP, a noise measurement is taken with the shutter in front of the TVAC optical port, from which the single-sample voltage noise for each pixel is computed as the standard deviation of a series of samples. The NEP is computed as the ratio between the voltage noise and the responsivity.

For a given bias setting, the responsivity is seen to decrease at the lower operating temperature, whereas for a given temperature of  $-10^{\circ}\text{C}$ , the responsivity increases from the 'low bias' to the 'high bias' test conditions. The bolometer pixel resistance is higher at the lower temperature and is the main contributing factor for the reduced responsivity at a given bias as this resistance appears at the denominator of the ROIC's integrator gain, which influences the detector system-level responsivity. For a given operating temperature (constant pixel resistance), it is the pixel-level responsivity that is increased in accordance with typical microbolometer behavior at the higher bias voltage [4]. It is further interesting to note the lower responsivity of pixel #26. This pixel was found to be modified by the presence of a foreign fibre observed during assembly and integration. The pixel performance is seen to be affected by this fibre (for example by potentially thermally bridging the pixel to the substrate, or by adding thermal mass to the pixel platform).

The single sample NEP is lower than 10 nW at the nominal operational temperature of  $-10^{\circ}\text{C}$ . The instrument application allows for averaging 77 samples for each measurement performed in flight (20-ms integration period). This averaging ensures that the NEP requirement of 3.7 nW is met for the EM detector under both bias conditions tested.

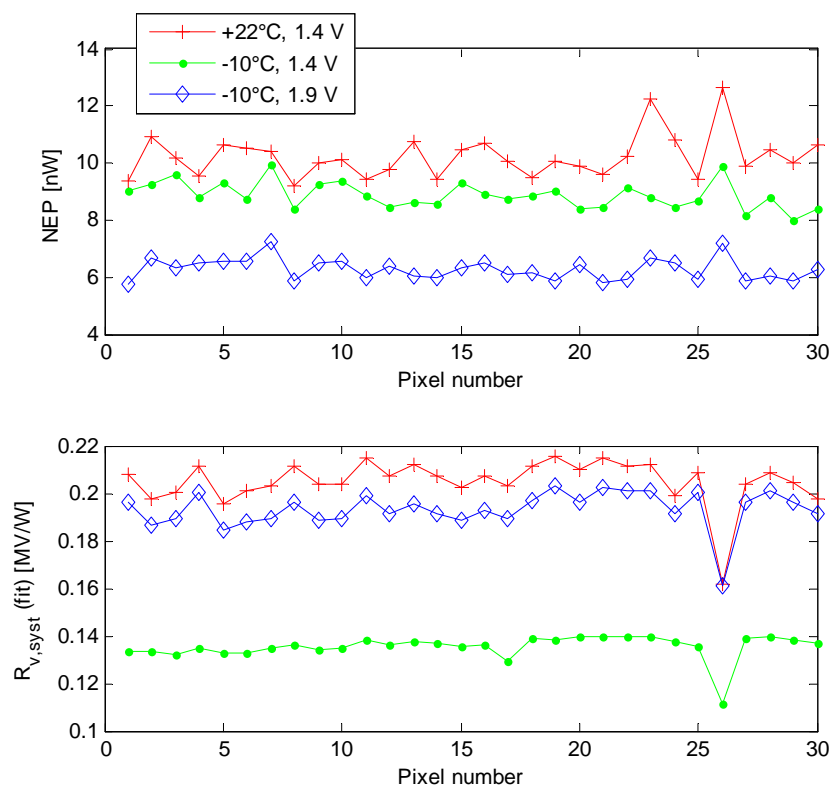


**Fig. 3.** EM detector NEP / responsivity measurements

The EM detector pixel time constant was also measured. For this measurement, the chopper frequency is varied between 10 Hz and 100 Hz and each pixel peak-to-peak response is recorded. A first-order filter equation is fitted over the experimental data to readily determine the pixel time constant. The measurement results showed that the time constant is only marginally affected by the different test temperature and bias conditions. In all cases, the time constant was below 5.5 ms, hence verified to be compliant with BBR's 6 ms requirement.

#### IV. DETECTOR QUALIFICATION PLANNING

Within the detector development programme, the next unit built will be the engineering qualification model (EQM). The performance of this unit will be fully characterized after being subjected to environmental tests, namely for sinusoidal (24 g) and random (14 g RMS) vibration testing, and for 8.5 thermal cycles under vacuum over the operational temperature range from -25°C to 45°C (including one excursion to the non-operating temperatures of -40°C and 50°C). The EQM will be validated for performance and visual inspection criteria before, during, and after the environmental tests.

The EarthCARE programme calls for the delivery of three Flight Models (FMs) as well as three fully characterized Flight Spares (FSs). All of these units will be tested according to an acceptance test campaign similar to the EQM qualification campaign; the principal difference will be that vibration tests and thermal cycling will be in accordance with the reduced levels and duration typical to such space programmes.

#### REFERENCES

- [1] K. Wallace, N. Wright, D. Spilling, K. Ward, and M. Caldwell, "The broadband radiometer on the EarthCARE spacecraft", *Proc. SPIE 7453*, paper no. 74530H, September 2009.
- [2] S. Ilias, P. Topart, C. Larouche, P. Beaupré, D. Gay, C. Proulx, T. Pope, and C. Alain, "Deposition and characterization of gold black coatings for thermal infrared detectors", in press.
- [3] C. Proulx, F. Williamson, M. Allard, G. Baldenberger, D. Gay, S. Garcia-Blanco, P. Côté, L. Martin, C. Larouche, S. Ilias, T. Pope, M. Caldwell, K. Ward, and J. Delderfield, "The EarthCARE broadband radiometer detectors", *Proc. SPIE 7453*, paper no. 74530S, September 2009.
- [4] P. W. Kruse, *Uncooled Thermal Imaging Arrays, Systems, and Applications*, SPIE press, pp. 34-40, 2001.